Available online at www.sciencedirect.com
ScienceDirect
Journal of Power Sources 164 (2007) 222–237
JOURNAL OF POWER SOURCES
www.elsevier.com/locate/jpowsour

Numerical study of water management in the air flow channel of a PEM fuel cell cathode

Peng Quan *, Ming-Chia Lai

Department of Mechanical Engineering, Wayne State University, Detroit, MI 48202, USA

Received 2 August 2006; received in revised form 9 September 2006; accepted 15 September 2006
Available online 27 November 2006

Abstract

The water management in the air flow channel of a proton exchange membrane (PEM) fuel cell cathode is numerically investigated using the FLUENT software package. By enabling the volume of fraction (VOF) model, the air–water two-phase flow can be simulated under different operating conditions. The effects of channel surface hydrophilicity, channel geometry, and air inlet velocity on water behavior, water content inside the channel, and two-phase pressure drop are discussed in detail. The results of the quasi-steady-state simulations show that: (1) the hydrophilicity of reactant flow channel surface is critical for water management in order to facilitate water transport along channel surfaces or edges; (2) hydrophilic surfaces also increase pressure drop due to liquid water spreading; (3) a sharp corner channel design could benefit water management because it facilitates water accumulation and provides paths for water transport along channel surface opposite to gas diffusion layer; (4) the two-phase pressure drop inside the air flow channel increases almost linearly with increasing air inlet velocity.

Keywords: Water management; PEM fuel cell; Air flow channel; Two-phase flow; Hydrophilicity; Pressure drop

1. Introduction

As one of the most promising technologies for auto transportation and power generation, proton exchange membrane (PEM) fuel cell has received great attentions from both academic institutions and industries due to its high efficiency, environmental friendliness, low working temperature, compact size, and rapid start-up feature. However, there remains much research and development work to make this energy conversion system more practical, durable, and economical for broader commercialization.

Water management is one of the critical issues for fuel cell design and optimization, and has been extensively studied both experimentally and numerically in the past decades. First of all, polymer membrane transferring the protons could only function well under fully saturated conditions in order to maintain good proton conductivity [1]. On the other hand, too much water may cause flooding at the electrodes thus blocking fuel and oxygen from reaching the reaction sites. In addition, excessive liquid water may also block the gas flow channel, or introduce unbalanced water distribution inside a cell or in different cells of a stack, thus affecting the reactant transport and decreasing the fuel cell performance. Water management inside gas flow channels can be optimized by reducing the liquid water coverage area on gas diffusion layer (GDL) surface, increasing drainage rate, minimizing pressure drop, etc. It is expected that significant performance gains and lifetime enhancement can be achieved with a better understanding of water transport phenomena inside PEM fuel cells.

For a single cell, water management could be considered in three sub-categories: water management in a proton exchange membrane, water management in gas diffusion layers, and water management in reactant flow channels. The first sub-category has been extensively studied since the beginning of 1990s and many numerical models regarding water management in membrane have been reported. The model proposed by Springer et al. [2] considered both electro-osmotic drag and diffusion of water through the membrane. They found that water transported through a membrane could be insignificant compared to the amount of water generated from the electrochemical reactions in a PEM fuel cell. In 1993, Nguyen and White [3] presented a steady, two-dimensional heat and mass transfer model for

* Corresponding author. Tel.: +1 313 577 0347; fax: +1 313 578 5943.
E-mail address: peng@eng.wayne.edu (P. Quan).

0378-7753/$ – see front matter © 2006 Elsevier B.V. All rights reserved.
doi:10.1016/j.jpowsour.2006.09.110

a PEM fuel cell. In this work, they considered liquid water transport through the membrane by electro-osmotic drag and diffusion and included the phase change of water. Recently, Cao and Djilali [4] studied the water management problem inside a membrane by applying conservation laws for water and current, in conjunction with an empirical relationship between electro-osmotic drag and water content, to obtain a transport equation for water molar concentration inside the membrane. The impacts of two-dimensionality, temperature, and pressure non-uniformities were analyzed and discussed.

Investigating water transport inside a porous GDL is not an easy task, neither by experiments nor by numerical simulations. So far, in situ experimental measurement of two-phase phenomena inside a porous GDL is still challenging and no detailed investigation was reported. In 2005, Litster et al. [5] conducted an ex situ visualization of liquid water transport in a PEM fuel cell GDL using fluorescence microscopy technique. In this experiment, fluorescein dye solution was pumped through the fibrous hydrophobic GDL and imaged with fluorescence microscopy. They found that liquid water transport through a porous GDL is only along a certain path, other than forming an "upside-down tree" capillary network. Neutron imaging and NMR microscopy techniques [6–13] seem very promising because of their non-intrusive nature and being capable of visualizing liquid water not only inside the gas flow channel but also in the porous GDL. In terms of numerical simulation, a GDL is usually mathematically described by using a porous media model, such as the work conducted by Li and Becker [14]. Essentially, a porous media model can be considered as a correction to the classical momentum conservation equation by adding a source term, which takes the effects of porous media on fluid flow into account. The drawback of using a porous media model is that the physically realistic pore structure cannot be considered explicitly.

Water management in gas flow channel is also very important. Bernardi and Verbrugge [15,16] and Springer et al. [2] investigated reactant transport through the GDL, but only vapor-phase water transport was considered in the gas flow channel. Recently, the study of water management in gas flow channel has been extended to two-phase. Zhang et al. [17] constructed a transparent single cell and by virtue of high-speed CCD camera, they observed the liquid water transport inside the gas flow channel and on the surface of the GDL as well. In this study, Liquid droplet formation and emergence from the GDL surface were characterized and liquid water removal mechanism from the GDL surface was identified. In addition, a theory was developed to determine what operating parameters and channel surface contact angles lead to sufficient liquid drainage from the fuel cell via corner flow. In 2005, Quan et al. [18] simulated the water behavior in a U-shaped air flow channel using volume of fraction (VOF) model in the FLUENT [19] computational fluid dynamics (CFD) package for the first time. In this work, five different cases with varying initial liquid water distribution were investigated. This work provided certain useful insights for understanding two-phase water behavior and introduced a new method for water management study in a PEM fuel cell. At the same time, Jiao et al. [20] did similar work for fuel cell stack with varying preset water distribution. Recently, Zhan et al. [21] conducted simulations to study droplet and film water motion in a flow channel of a PEM fuel cell using the same approach but the hydrophilicity of graphite plate and the hydrophobicity of the gas diffusion layer surface were taken into account. A common problem of all these works involving VOF model is that the liquid water must be placed a priori somewhere inside the computation domain, which makes the simulation less physically realistic and also makes the quasi-steady-state simulation, which provides important insight to the processes, unachievable.

In the following section, the model assumptions and formulations, boundary conditions, as well as the grid independency validation are summarized. Next, the effects of channel surface hydrophilicity, channel geometry, and air inlet velocity on water behavior, water content inside the channel, and two-phase pressure drop are discussed in detail. Finally, in Section 4, conclusions from the numerical study are drawn.

2. Numerical model and boundary conditions

2.1. Model assumptions

To simplify the study, the following assumptions were invoked:

(a) isothermal condition—no temperature variation was considered in the simulations;
(b) no detailed electrochemical mechanism considered. Since no reaction takes place in the gas flow channel and GDL, the current problem could be simplified to a two-phase fluid mechanics problem with air flow and liquid water source applied on boundaries;
(c) product water generated through electrochemical reactions and the water transported from membrane are at liquid phase and the total water flux is assumed constant;
(d) no water phase change is considered;
(e) the GDL is modeled as homogenous porous media without considering detailed pore structure.

2.2. Physical and computation domain

As one of the major aspects concerning water management, a simulation of water behavior inside an air flow channel would be incomplete without including the porous gas diffusion layer. In this study, as shown in Fig. 1, a U-shaped air flow channel (1 mm × 0.5 mm × 23 mm) was attached to a layer of porous media (GDL, such as carbon paper) of 0.2 mm thickness. This computation domain can be understood as a basic assembly element isolated from a very complex gas flow channel configuration. Thus the information obtained from this simulation would provide useful insights for bipolar plate design and optimization.

2.3. Boundary conditions

For this 3D two-phase flow simulation, no-slip boundary condition was applied to all the three interior walls of the channel.

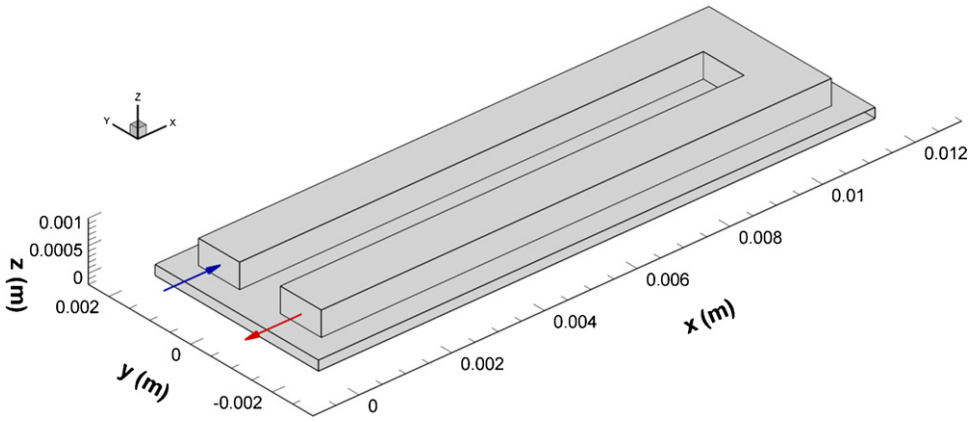

Fig. 1. Computation domain: a U-shaped gas flow channel with sharp corners attached to a porous GDL.

The wall adhesion effects can be taken into account by assigning different contact angles according to varying channel material specifications. A velocity inlet boundary condition, which could vary for different cases, and an outlet boundary condition were applied at the channel inlet and the outlet, respectively, to simplify duct entrance and outflow boundary effects. In this study, the inlet air flow velocity varied from 1.43 to 7.15 m s^{-1}, corresponding to flow stoichiometric ratio of 2 (commonly used in PEM fuel cell operation) and 10 at the working condition of current density of 0.8 A cm^{-2}, cell temperature of 80 °C, and pressure of 2 atm, respectively.

On the bottom surface of the GDL, a constant liquid water mass flux boundary condition was applied. According to [22], the water flux at the GDL–catalyst layer interface can be given as

$$N = \frac{M(1+2\alpha)i}{2F} \tag{1}$$

where M the molecular weight (18 g mol^{-1} for water), α the net water transport coefficient in the membrane (a constant of 0.1 in this study). i is the fuel cell operating current density (0.8 A cm^{-2}) and F is the Faraday constant, 96,487 C mol^{-1}. Evidently, the water flux considers both oxygen reduction reaction and water transport from the membrane. The liquid water flux throughout the simulations was set to 0.0895 kg s^{-1} m^{-2}.

It should be pointed out that since the water generation rate inside an operating PEM fuel cell is quite slow, its numerical value under the previously mentioned working condition (0.000895 kg s^{-1} m^{-2}) was amplified two orders of magnitude to shorten the water accumulation stage inside the GDL and to facilitate the two-phase flow visualization inside the channel. In fact, for the quasi-steady-state processes investigated in this study, the water distribution, water content inside the channel, and pressure drop are functions of channel geometry, channel surface wettability, and inlet air flow rate, as well as water generation rate. Considering the fact that the amount of liquid water inside the channel is quite small (as shown in Section 3), the unrealities introduced by the amplified water generation rate are not significant. Therefore, the simulations are still capable of providing qualitative guidance for PEM fuel cell design and optimization.

2.4. Computational methodology

A commercial CFD software package, FLUENT, was used to perform the simulations. Based on the conservation equations of mass and momentum, and a transport equation for volume fraction, the two-phase flow problem can be systematically solved for different working conditions by incorporating different boundary conditions.

Continuity equation:

$$\frac{\partial \rho}{\partial t} + \nabla(\rho \vec{v}) = 0 \tag{2}$$

Momentum equation:

$$\frac{\partial(\rho \vec{v})}{\partial t} + \nabla(\rho \vec{v}\vec{v}) = -\nabla p + \nabla(\bar{\bar{\tau}}) + \rho \vec{g} + \vec{F} \tag{3}$$

where p is the static pressure, $\vec{F}$ a momentum source term, which includes terms caused by surface tension and porous effects. $\bar{\bar{\tau}}$ is the stress tensor given by

$$\bar{\bar{\tau}} = \mu(\nabla \vec{v} + \nabla \vec{v}^{\mathrm{T}}) - \frac{2}{3}\mu \nabla \vec{v} I \tag{4}$$

where μ is the dynamic viscosity and I is the unit tensor.

For the current fuel cell simulations where a simple homogeneous porous media (porosity $\varepsilon = 0.8$) is assumed and the flow regime is laminar, a source term (part of the source terms, $\vec{F}$, in momentum equations) due to porous media effects is added to the classical Navier-Stokes equation and it is in the form of

$$\vec{S} = -\frac{\mu}{\kappa}\vec{v} \tag{5}$$

where κ is the permeability of the porous material and $1/\kappa$ is usually termed viscous resistance coefficients (a value of 1×10^{12} m^{-2} was adopted throughout the simulations in this study).

Liquid water and air were considered as two immiscible fluids. Therefore, the volume of fluid (VOF) model implemented in the FLUENT [19] can be adopted to capture the dynamic interface between them. In the VOF model, the basic continuity equation for the volume fraction, F, is solved first; then the reconstruction of the interface throughout the computation domain is performed in a post-processing fashion. For the ith phase, the

volume fraction equation without considering source term and inter-phase terms has the following form:

$$\frac{\partial}{\partial t}(F_i\rho_i) + \nabla(F_i\rho_i v_i) = 0 \quad (6)$$

The volume fraction for the primary phase (air in the present study) can be computed based on the following constraint:

$$\sum_{i=1}^{n} F_i = 1 \quad (7)$$

The surface tension along the air–water interface and wall adhesion play important roles in a two-phase transport process in a micro-channel. In the FLUENT, a widely used surface tension model, the continuum surface force (CSF) model, proposed by Brackbill et al. [23] is adopted. Originally the CSF model is based on the force balance between the pressure drop across the two phases and the surface tension along the surface. With this model, the consideration of surface tension results in a portion of the source term, $\vec{F}$, in the momentum Eq. (3). Additionally, effects of wall adhesion can be taken into account by specifying a wall adhesion angle (contact angle) in conjunction with the CSF model in the FLUENT. Numerically, rather than imposing this boundary condition on the wall itself, the contact angle that the fluid is assumed to make with the wall is used to adjust the surface normal in cells near the wall, thus resulting in the adjustment of the interface curvature close to the wall. More detailed information can be found in [19]. It is worth mentioning that the default value for wall contact angle of 90° was used for the GDL walls and besides, a constant air–water surface tension of 0.0662 N m^{-1} was adopted throughout this study.

2.5. Validation of grid independency

For the simulation involving U-shaped channel with sharp corners, a 3D structured orthogonal grid with 7885 computation nodes was employed (an unstructured mesh with 8549 nodes for the round corner case). The grid independency was validated by performing computations for the baseline case (as listed in Table 1 below), using three meshes with different node numbers. The resulting liquid water distributions for the three cases are quite consistent, so the mesh with 7885 nodes was used throughout this study.

Table 1
Five simulation cases for the U-shaped channel (sharp corner) with varying hydrophilicity

Case #	Velocity (m s^{-1})	Contact angle (°)	Corresponding hydrophilicity
1	1.43	0	Hydrophilic (complete wetting)
2	1.43	45	Hydrophilic (partial wetting)
3[a]	1.43	90	N/A (no wall adhesion)
4	1.43	135	Hydrophobic (partial non-wetting)
5	1.43	180	Hydrophobic (negligible wetting)

[a] Baseline case for this study.

3. Results and discussions

The simulations performed in this study are capable of revealing unsteady features of the air–water flow in the channel. Fig. 2, a plot from our simulation results, shows a typical time history for water content, which is defined as the volume integral of volume fraction for liquid phase. At time $t = 0$, liquid water generation starts from the bottom surface of the GDL and the whole GDL layer is fully occupied by liquid water at $t = 1.2$ s. From $t = 1.2$ to 1.75 s, a steep increase of water content inside the channel can be observed. This corresponds to the process of establishing a quasi-steady state. After $t = 1.75$ s, the level of water content remains relatively stable. This quasi-steady state indicates that the water generated is balanced by the drainage from the channel. Since, in most of the time, fuel cells operate under a relatively stable condition, the quasi-steady working condition characterized by the horizontal portion in Fig. 2 is our focus throughout this study.

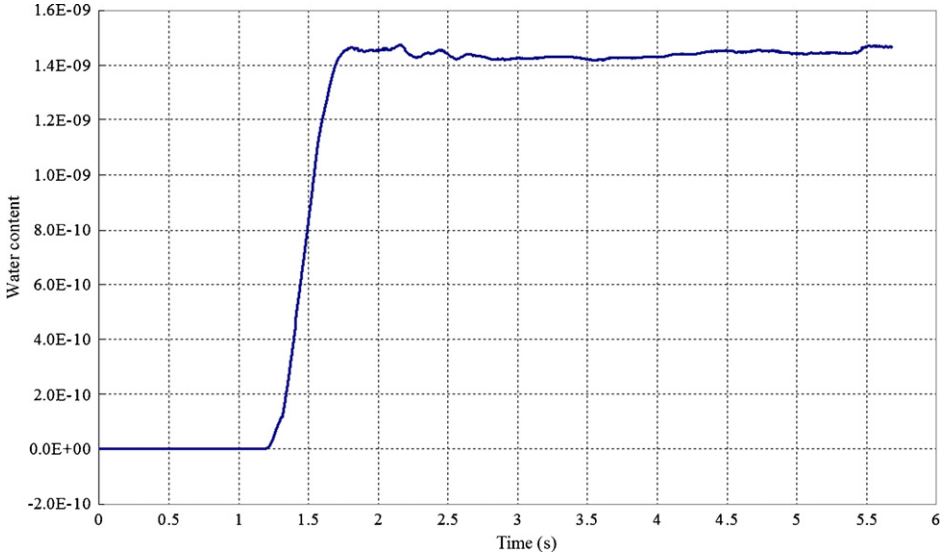

Fig. 2. Water content in gas flow channel vs. time for a typical unsteady process.

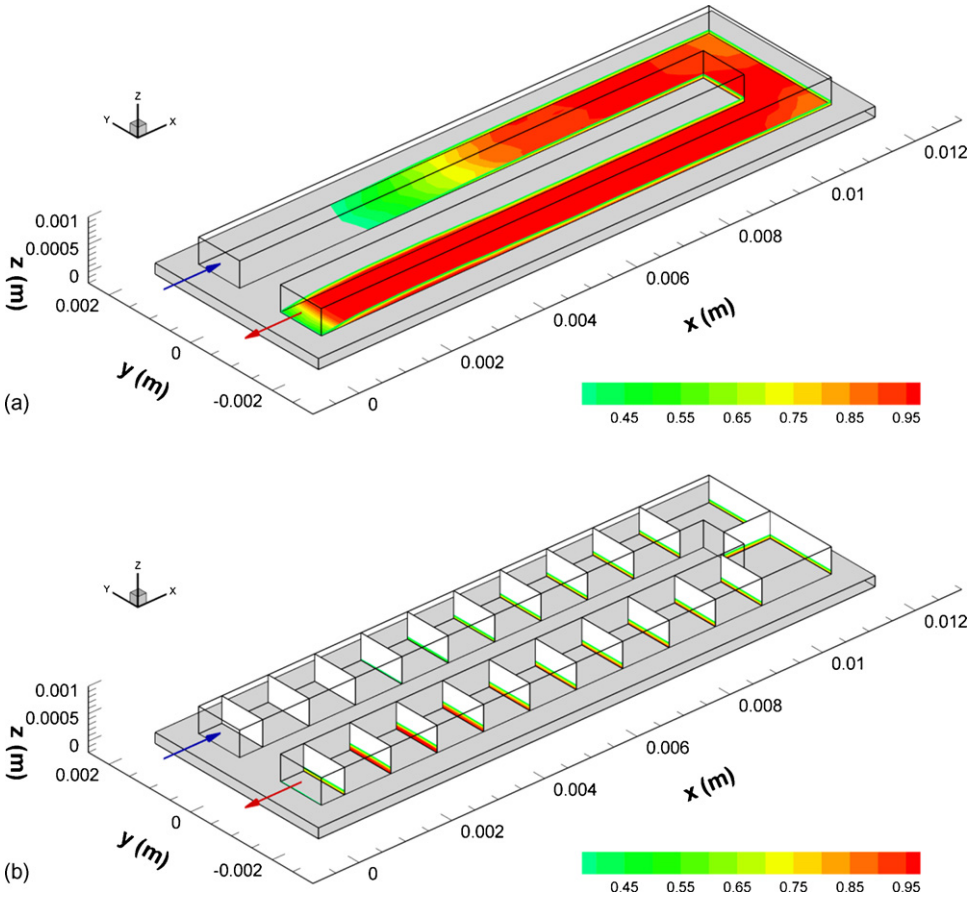

Fig. 3. Liquid water distribution for the baseline case (1.43 m s^{-1}, 90°, and sharp corners): (a) overall liquid phase distribution; (b) water distribution on selective cross-sections.

As for water behavior in GDL, it could be investigated only if the detailed physical structure and properties of the porous media were taken into account. For the porous media model used in this study, the uniformly distributed liquid phase provides no valuable information in term of free surface tracking, thus being invisible in the following discussions for the purpose of clarity.

3.1. Effects of channel surface hydrophilicity on water behavior, water content, and pressure drop

To investigate the effects of channel surface hydrophilicity on water management, five different contact angles were chosen to perform the parametric study. These cases were summarized in Table 1.

3.1.1. Effects of channel surface hydrophilicity on water behavior

All cases in this subsection are for a PEM fuel cell working at a relatively low gas inlet velocity (1.43 m s^{-1}). By changing contact angles of the three channel wall surfaces, different water behaviors can be observed. For the baseline case (contact angle of 90°), a typical water distribution inside the channel is shown in Fig. 3. Fig. 3a shows the overall liquid water distribution. Ignoring the channel entrance, a layer of liquid water with nearly uniform thickness covers the whole GDL surface. This is also clearly demonstrated in Fig. 3b, water distribution at several selective cross-sections. The simulation indicates that, at contact angle of 90°, water drainage takes place along the edges near the GDL surface and gas flow channel surfaces are of no help with water management. Obviously, this is not an optimized design.

Now decreasing the contact angle to 45°, a partial wetting condition, the corresponding water distribution is given in Fig. 4. Compared with the baseline case, certain amount of water (droplets) is being removed through periodical corner flow along the outer upper edge. Along the lower edges, large amount of water removal is achieved through a continuous corner flow and it can be seen that this portion of water is prone to climbing up onto the side wall and spreading to form a larger contact area when flowing to the exit. This is obviously due to the hydrophilic feature of the channel surfaces. In addition, the droplets grow in size when moving along the upper edge, by combining with the latish formed ones. These larger droplets cannot retain at their original position since the enlarged surface endures larger shear stress from air flow and the increasing net force drags the enlarging droplets to the exit of the channel. Another point distinguishing from the baseline case is that the GDL flood-coverage area reduces significantly, as shown in both Fig. 4a and b. It also should be pointed out that, in reality, the area would be even smaller if the hydrophobic feature of the GDL surface were considered.

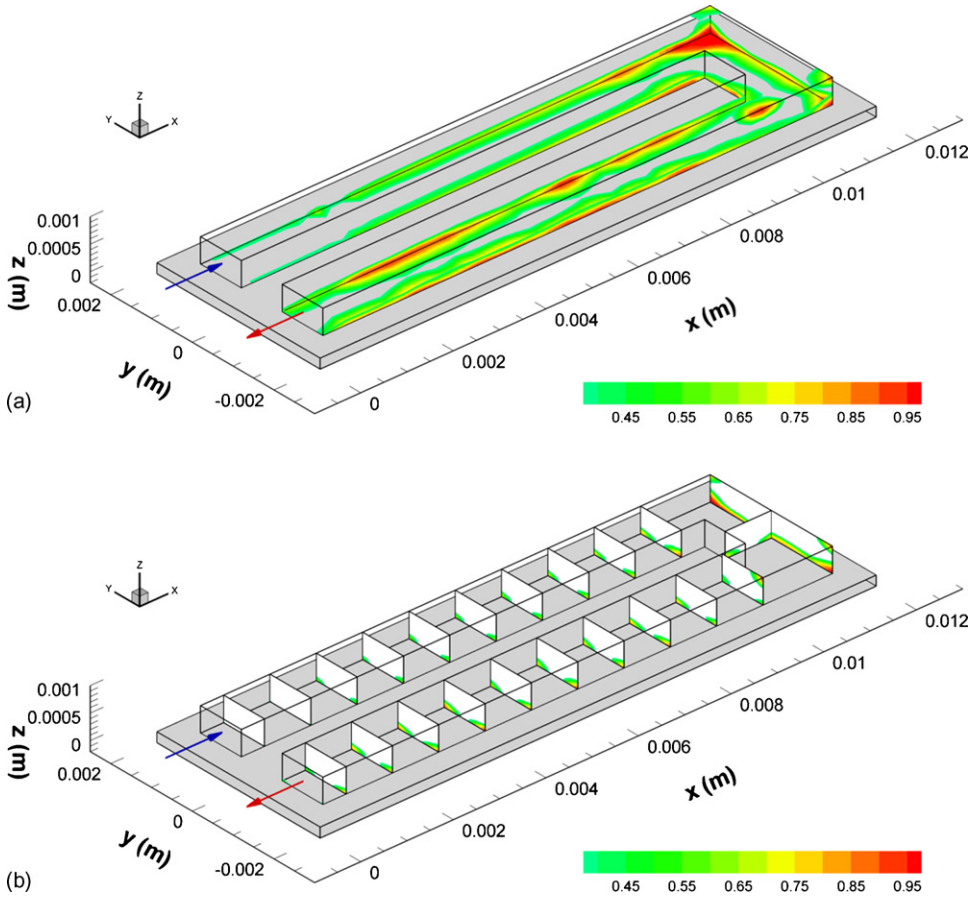

Fig. 4. Liquid water distribution for case #2 (1.43 m s^{-1}, 45°, and sharp corners): (a) overall liquid phase distribution; (b) water distribution on selective cross-sections.

Interestingly, the liquid water behavior observed in case #2 can be validated since it is quite consistent with some experimental observations published in open literature. For instance, in [17], liquid water distributions in air flow channel at different working conditions were captured by using a CCD camera and it was found that corner flow is an important water removal mechanism when air velocity is low.

The complete wetting condition can be achieved by further decreasing the contact angle to 0° and one set of figures corresponding to this case are given in Fig. 5. Compared with the case of 45°, larger amount of water being removed along the upper outer edge can be observed and the velocity of water motion becomes higher. In addition, the liquid water coverage area on GDL surface further decreases, which is beneficial to reactant transport to the reaction sites by providing more effective area. An interesting phenomenon is observed in this simulation: almost no water droplets or films can be observed along the upper edge before the bend, which is quite contrary to the situation in the after-bend portion. In the liquid recirculating zones around the sharp corners, liquid water accumulates and gradually piles up and eventually reaches the upper surface of the channel. It is the liquid recirculating zones at the sharp corners that provide effective paths for the liquid water to climb up onto the upper edges, thus leaving more valuable effective area on the GDL surface for reactant transport.

What will happen in terms of water behavior if the material of bipolar plate to be chosen is hydrophobic? Figs. 6 and 7 are simulation results for the case of 135° and 180°, respectively, which are quite similar. They show that in the case of using hydrophobic material, liquid water is prevented from touching the channel surfaces, resulting in almost no drainage flows along the lower edges. As a result, most of the GDL surface is covered by a layer of liquid water with a parabolic cross-sectional shape, which forms a barrier to reactant transport to GDL. Obviously, this is the case that should be avoided in selecting bipolar plate materials.

Please note that if the hydrophobicity and the detailed physical structure of GDL surface were taken into account, some additional information regarding water behavior would be available. For example, the droplet formation on the GDL surface may be observed at lower air velocity [24]; and at a higher air velocity a mist flow could be the flow regime for liquid water removal [17].

3.1.2. Effects of surface hydrophilicity on water content inside the channel

Fig. 8 is a plot of water content history (inside the channel only) for all the five cases listed in Table 1. The water content inside the channel oscillates within a small range for each case. The most stable one is for contact angle of 90° but the water content is also the most. The water content values oscillate more

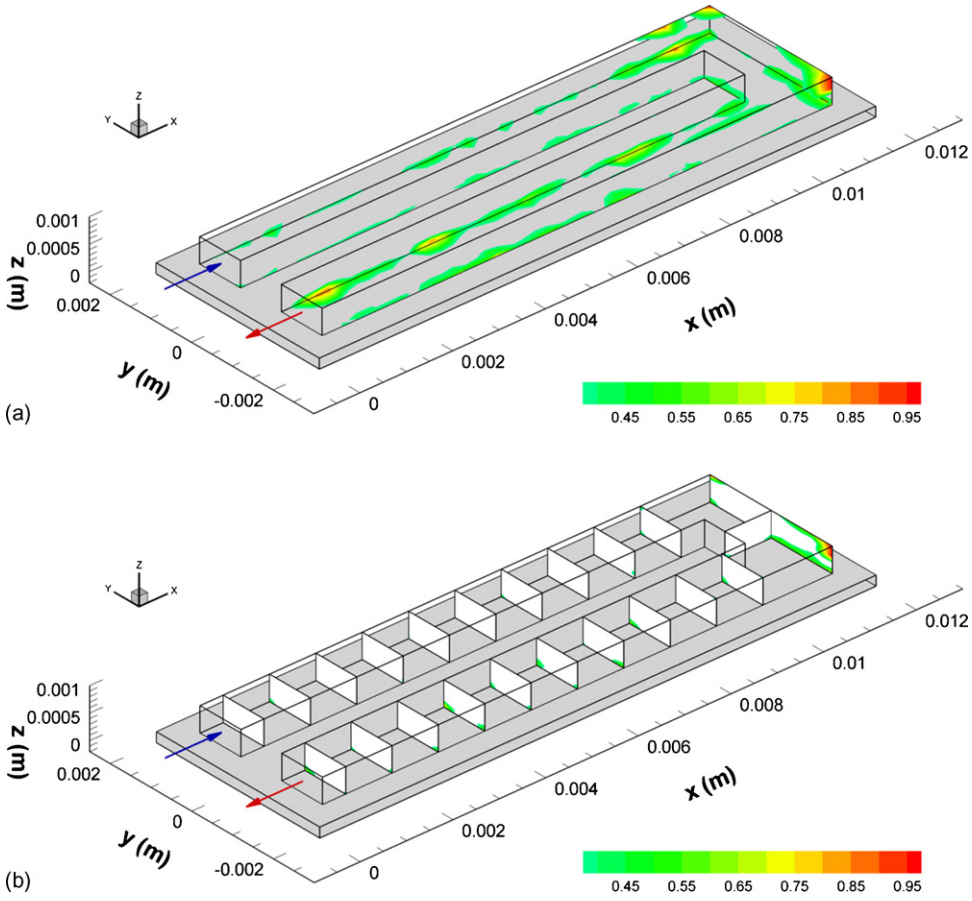

Fig. 5. Liquid water distribution for the case #1 (1.43 m s^{-1}, 0°, and sharp corners): (a) overall liquid phase distribution; (b) water distribution on selective cross-sections.

significantly for all the other four cases, since the water transport in these cases is more active compared with the 90° case.

The plot of average water content vs. contact angle (Fig. 9) indicates that, for the 90° case, it holds the most water, nearly doubles that of the 180° case. An effective drainage strategy requires the water being removed as timely as possible and the water content in gas flow channels as less as possible. Therefore, the material selection in a bipolar plate design should be away from the peak area as shown in Fig. 9.

3.1.3. Effects of surface hydrophilicity on pressure drop inside the channel

A better understanding of the relation between pressure drop and two-phase flow in side the gas flow channel is of importance for fuel cell system design because the two-phase flow characteristics in a micro-channel are significantly different from those of larger scales, which have been extensively studied since 1970s. Based on the simulation results obtained, the relationship between pressure drop and surface contact angle is briefly discussed in the following section.

Fig. 10 shows the pressure drop history for the five cases. A steady-state single-phase (air only) pressure drop line was added to the figure as well. Comparing with the pressure drop for the single-phase case, the increase of pressure drop due to the addition of liquid phase is quite significant. The increased pressure drop is attributed to (1) the blockage effect due to added liquid water; (2) wave drag effect introduced by the liquid water spreading on the channel wall surfaces. According to the simulation, the two-phase pressure drop should be in the range of 1.5–2.3-fold of its single-phase counterpart.

It can also be observed from Fig. 11, plot of average two-phase pressure drop vs. contact angle, that for a hydrophilic channel surface, the pressure drop decreases significantly as the contact angle increases. This is mainly due to the spreading area on the channel surface reduces with increasing contact angles, thus weakening the wave drag effect, as shown through Fig. 4a and 5a. In other words, the larger contact angle, the smaller water spreading area on the channel surface, thus the smaller drag force (interfacial tension) would exert on the gas flow, resulting in a decreased pressure drop. However, when the channel surface becomes more hydrophobic (contact angle greater than 90°), the pressure drop becomes much more constant. This attributes to the fact that, when the contact angle becomes greater than 90°, liquid water is pushed away from channel surfaces, making the water flow a liquid film on the GDL surface; it can be seen that this liquid film is quite stable, and provides less contact area with the air flow, as shown in Fig. 3a and b, 6a and b, and 7a and b. Therefore, we conclude that a hydrophilic channel surface is preferable, but it would induce a significant pressure drop inevitably.

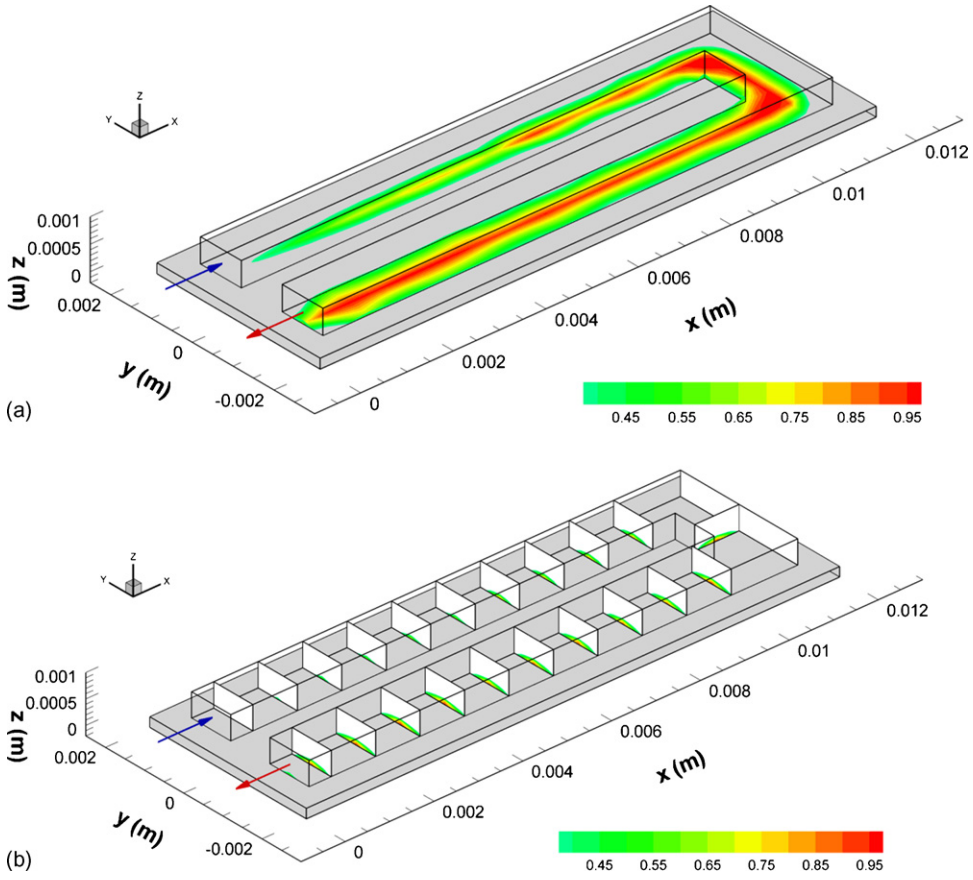

Fig. 6. Liquid water distribution for case #4 (1.43 m s^{-1}, 135°, and sharp corners): (a) overall liquid phase distribution; (b) water distribution on selective cross-sections.

3.2. *Effects of channel geometry on water behavior, water content, and pressure drop*

In this section, two cases of different geometries: the previously used U-shaped channel with sharp corners and another one with round corners (shown in Fig. 12), are used to investigate the effects of channel geometry on water behavior, water content, and pressure drop. The parameters for the simulations using the round corner geometry are given in Table 2.

3.2.1. *Effects of channel geometry on water behavior*

When contact angle is set to 90°, the simulation results for the two cases with different geometries show no significant difference in terms of water behavior. The overall GDL surface is covered by a layer of liquid water for both cases. No water transport along the top or side surfaces can be observed. The water distribution for the round corner case is given in Fig. 13, and that for the sharp corner geometry can be found in Fig. 3a.

However, when contact angles are set to 45°, corresponding to the case of a moderate hydrophilic channel surface, the difference becomes significant. Fig. 14 shows the water distribution for this case where liquid water in the bend flows strictly along the lower edge (the lower semicircle) and none of it is capable of climbing up onto the side wall and touching the upper surface. The difference attributes to geometry. For the sharp corner case, large amount of water accumulates in the recirculating zones (at the sharp corners) and it gradually piles up and reaches the upper surface of the channel. After that, this portion of water leaves the channel by means of periodical corner flow along the upper edge, as shown in Fig. 4a. However, for the round corner case, the flow field in the bend is streamlined by the round corners; and no significant liquid recirculating zones can be observed in the bend area. This prevents the liquid water from accumulating and piling up, eventually forming corner flows along the lower outer edge only. It is noticeable that, inside the bend, most of the GDL surface is covered by liquid water, in contrary to the sharp corner case where less GDL surface is. Therefore, the consideration of sharper corners when designing a gas flow channel may be of benefit for water management because it provides paths for the liquid water to the upper surface, thus saving more valuable effective GDL surface area for reactant transport.

Table 2
Two simulation cases for the U-shaped channel with round corners

Case #	Velocity (m s^{-1})	Contact angle (°)	Corresponding hydrophilicity
6	1.43	45	Hydrophilic (partial wetting)
7	1.43	90	N/A (no wall adhesion)

3.2.2. *Effects of channel geometry on water content*

Fig. 15 is the plot of water content history (inside the channel only) for four cases indicated in the figure. It can be observed that, in general, the water content for a round corner design is less than that for its sharp corner counterpart. The main reason

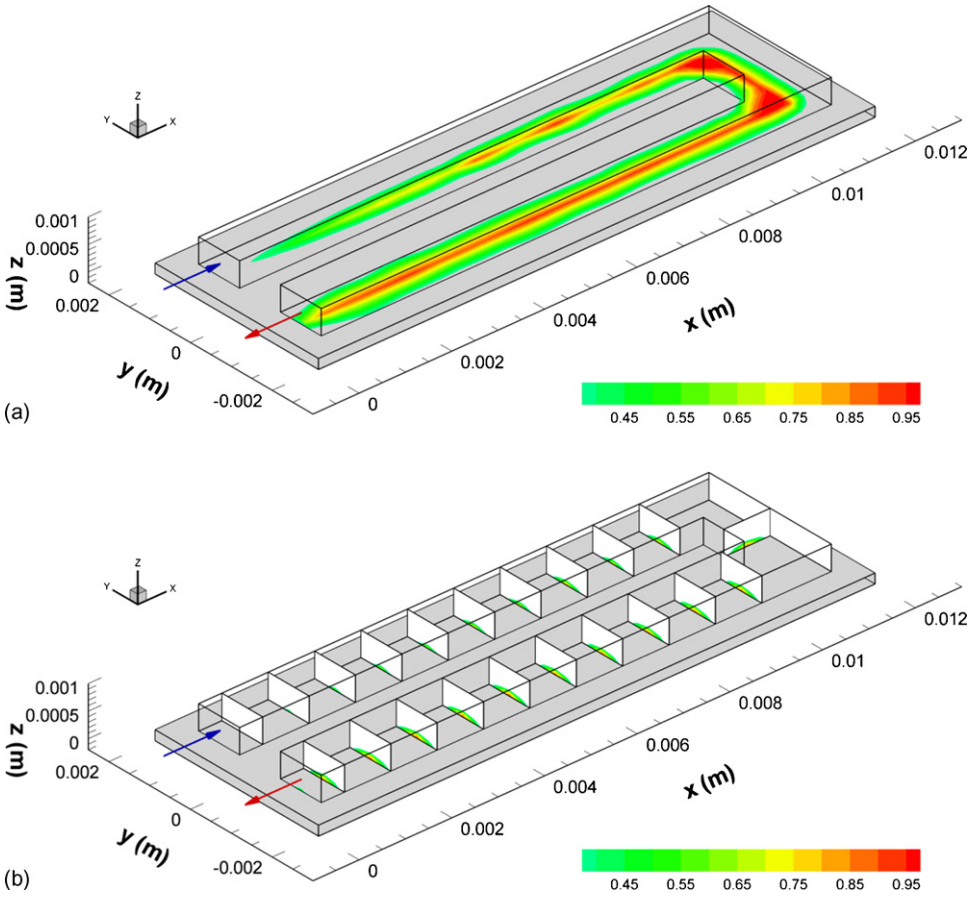

Fig. 7. Liquid water distribution for case #5 (1.43 m s^{-1}, 180°, and sharp corners): (a) overall liquid phase distribution; (b) water distribution on selective cross-sections.

is that the recirculating zones at the sharp corners retain more water than that of a smooth, streamlined round corner design.

3.2.3. *Effects of channel geometry on pressure drop*

The effects of channel geometry on pressure drop are not remarkable for these lower air velocity simulations. Only a slight difference can be observed from the pressure drop history as shown in Fig. 16. Generally, the pressure drop for the sharp corner cases is slightly higher than that for the round corner cases. And this trend is quite consistent with the single-phase cases, which are shown by two straight lines at the bottom of this figure.

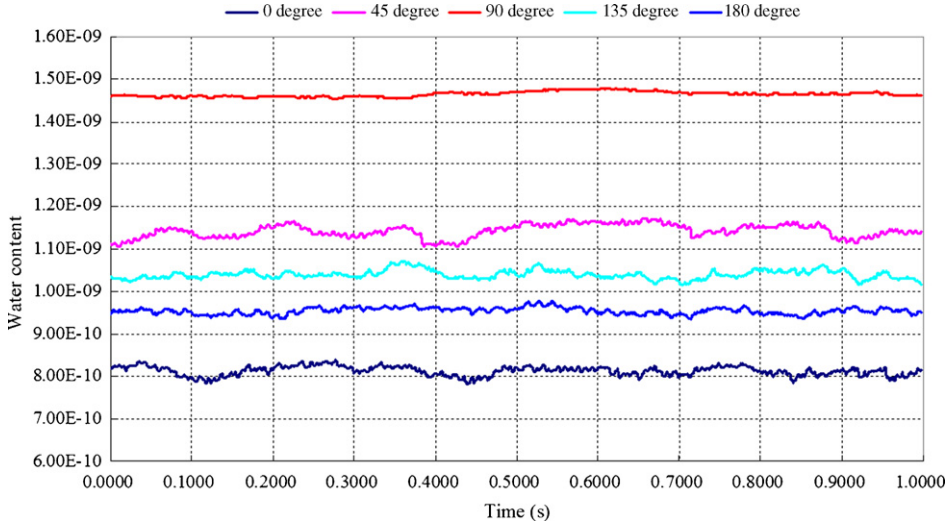

Fig. 8. Water content history (inside the channel only) for all the five cases of varying channel surface hydrophilicities.

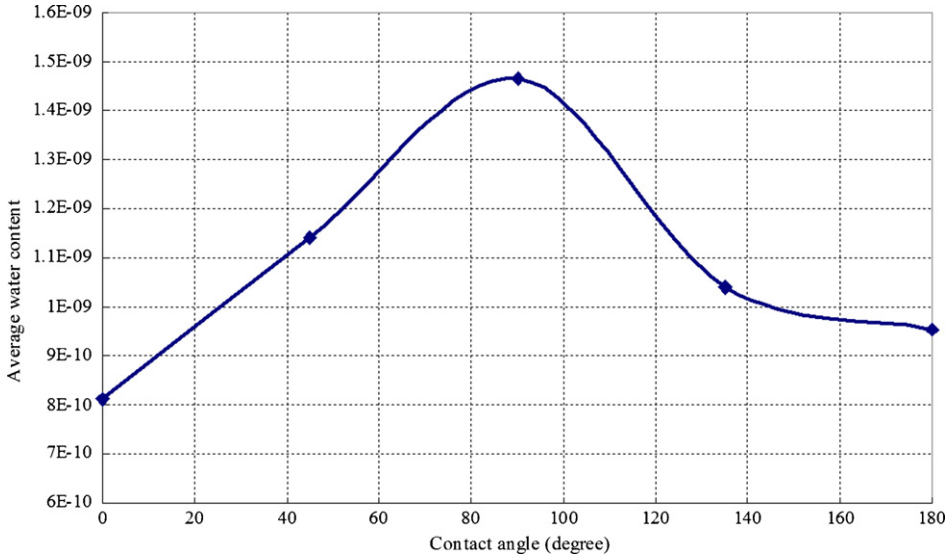

Fig. 9. Average water content vs. contact angle.

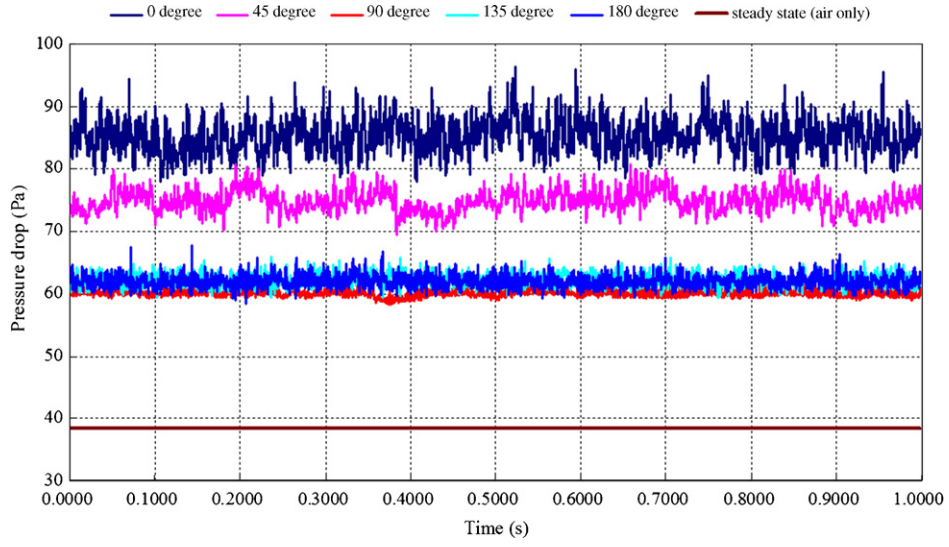

Fig. 10. Two-phase pressure drop along the channel for all five cases of varying channel surface hydrophilicities.

3.3. *Effects of inlet air velocity on water behavior, water content, and pressure drop*

For different operating conditions of a PEM fuel cell, the air velocity at the inlet could vary. To investigate the effects of inlet gas velocity on water behavior, water content, and two-phase pressure drop, the following four cases (listed in Table 3) with varying gas inlet velocities were numerically simulated. Combining with case #2, these simulations cover the range of inlet velocity from 1.43 to 7.15 $m\,s^{-1}$, providing a detailed description of the relationship between inlet gas velocity and two-phase flow in the reactant flow channel. Note that these inlet velocities correspond to the Reynolds numbers ranging from 66 to 329, provided a single-phase Reynolds number based on the air flow at the channel inlet is considered.

Table 3
Four simulation cases for the U-shaped channel with sharp corners at higher air inlet velocity

Case #	Velocity ($m\,s^{-1}$)	Contact angle (°)	Corresponding stoichiometric ratio	Corresponding inlet air Reynolds number
8	2.86	45	4	132
9	4.29	45	6	197
10	5.72	45	8	263
11	7.15	45	10	329

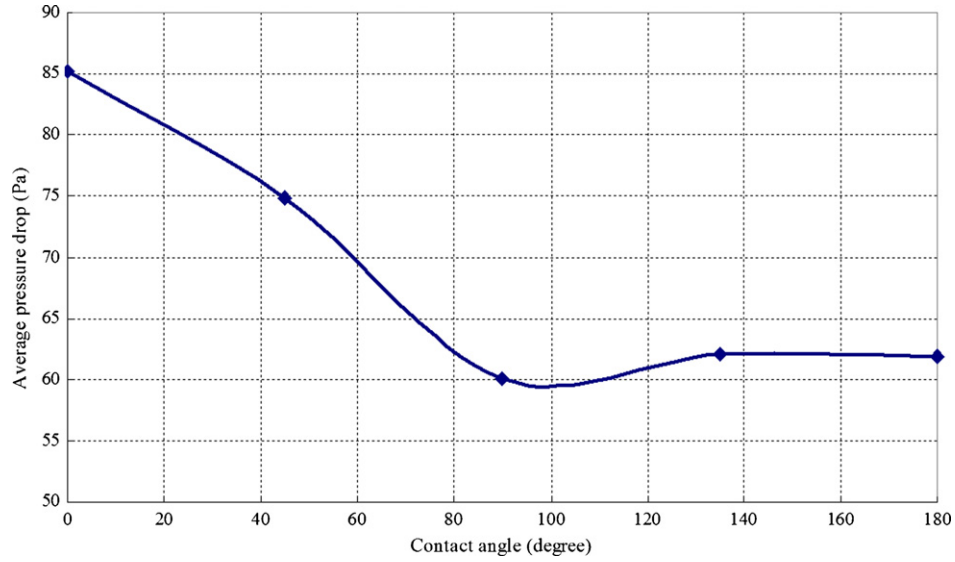

Fig. 11. Average two-phase pressure drop vs. contact angles.

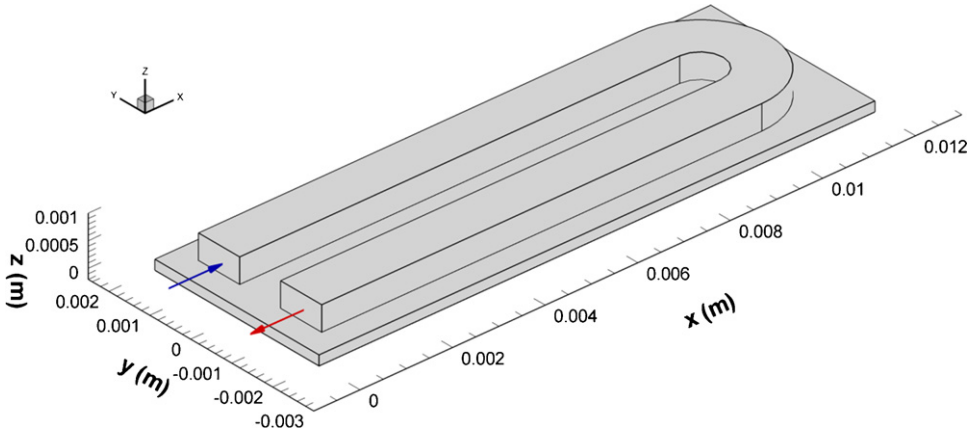

Fig. 12. A U-shaped channel with round corners attached to a GDL.

3.3.1. Effects of inlet gas velocity on water behavior

Fig. 17 shows the water distribution inside the air flow channel under the condition of inlet velocity varying from 2.86 to 7.15 m s^{-1}. Clearly, the water distribution is affected by the increasing gas velocity because the interfacial tension becomes more significant. It can be observed that the flow regime at 2.86 m s^{-1} is quite similar to the case of 1.43 m s^{-1} (case #2). All phenomena, such as water accumulation, water-climbing-up,

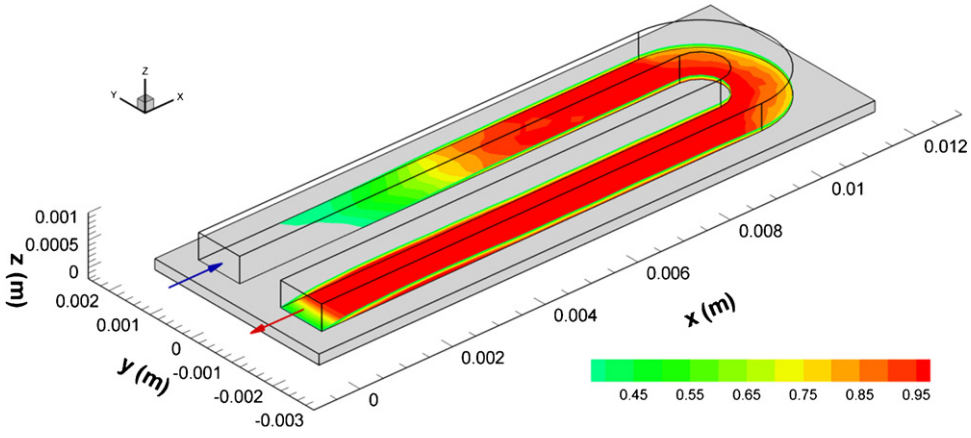

Fig. 13. Liquid water distribution for case #7 (1.43 m s^{-1}, 90°, and round corners).

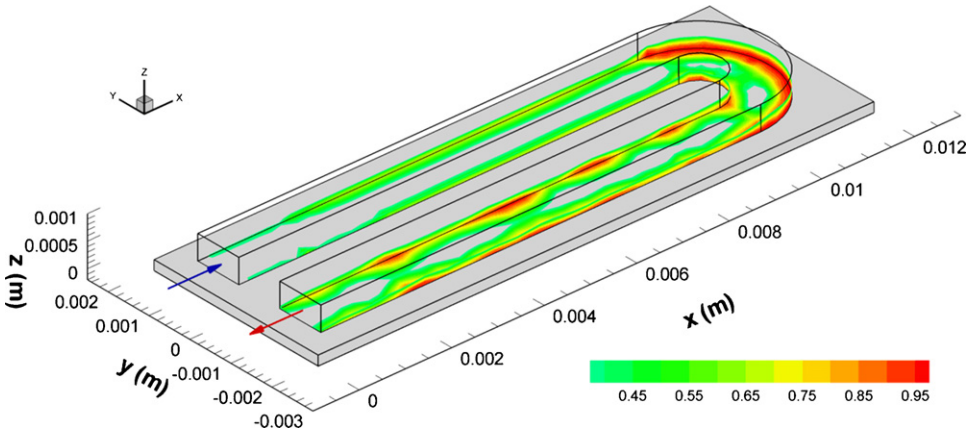

Fig. 14. Liquid water distribution for case #6 (1.43 m s^{-1}, 45°, and round corners).

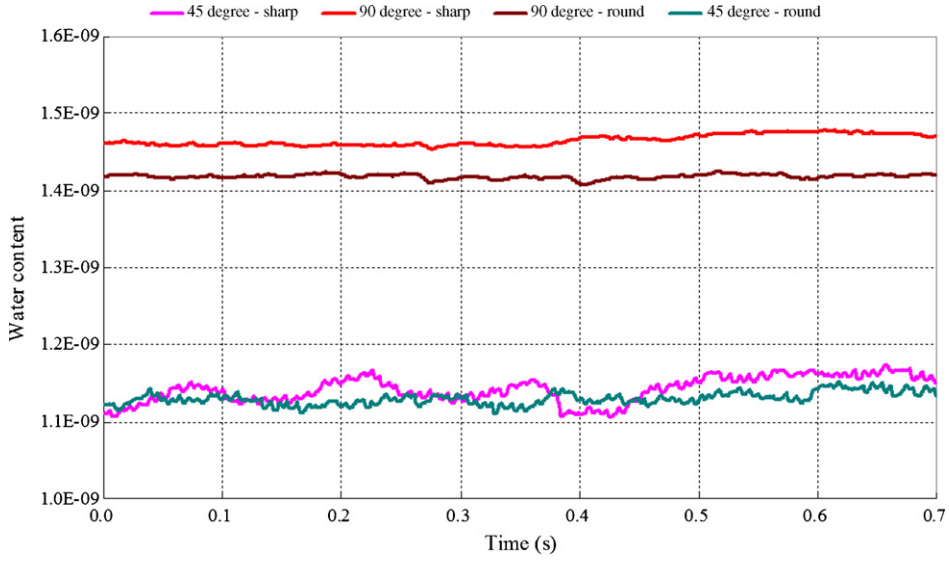

Fig. 15. Water content history for four cases involving different hydrophilicities and geometries.

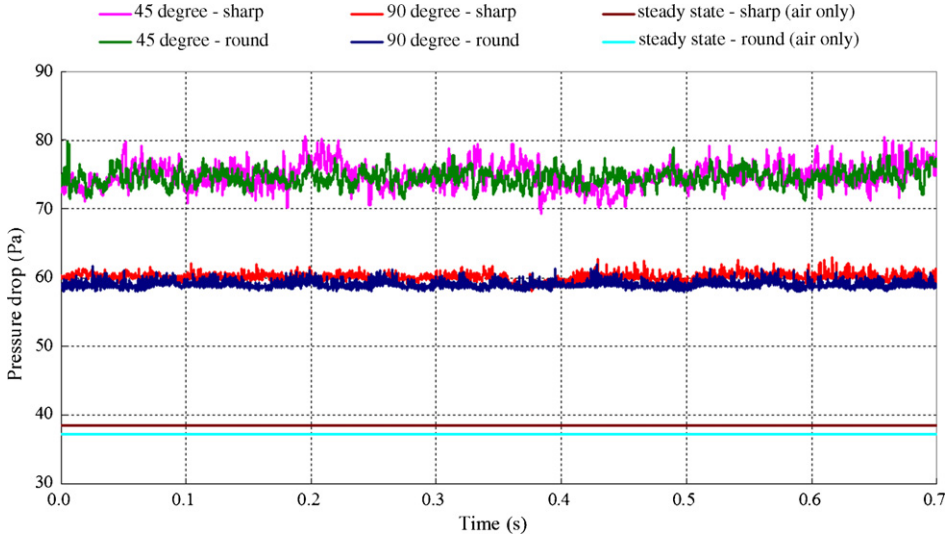

Fig. 16. Pressure drop for cases involving different hydrophilicities and geometries.

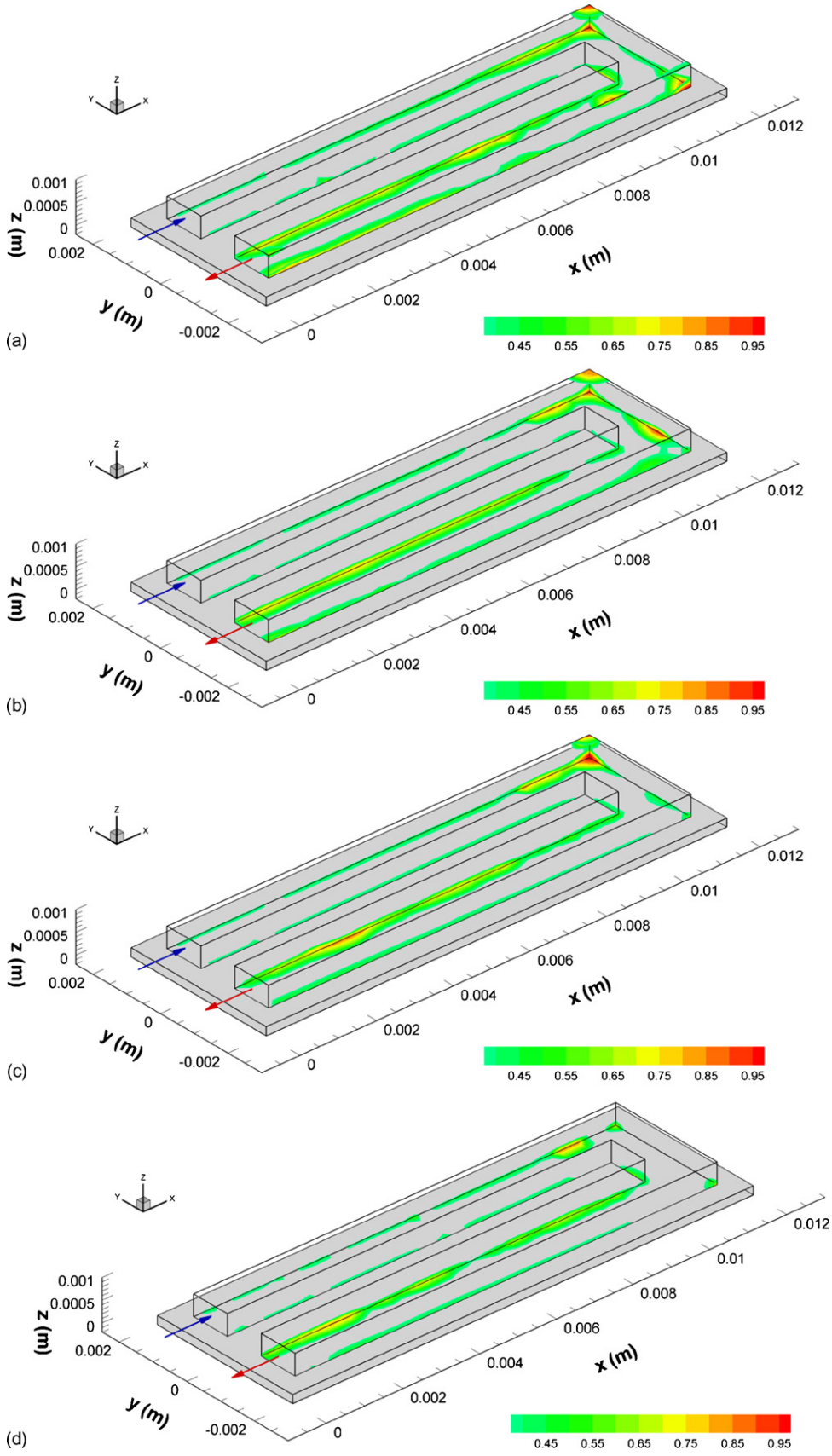

Fig. 17. Liquid water distribution for cases with varying air inlet velocity: (a) 2.86 m s^{-1}; (b) 4.29 m s^{-1}; (c) 5.72 m s^{-1}; (d) 7.15 m s^{-1}.

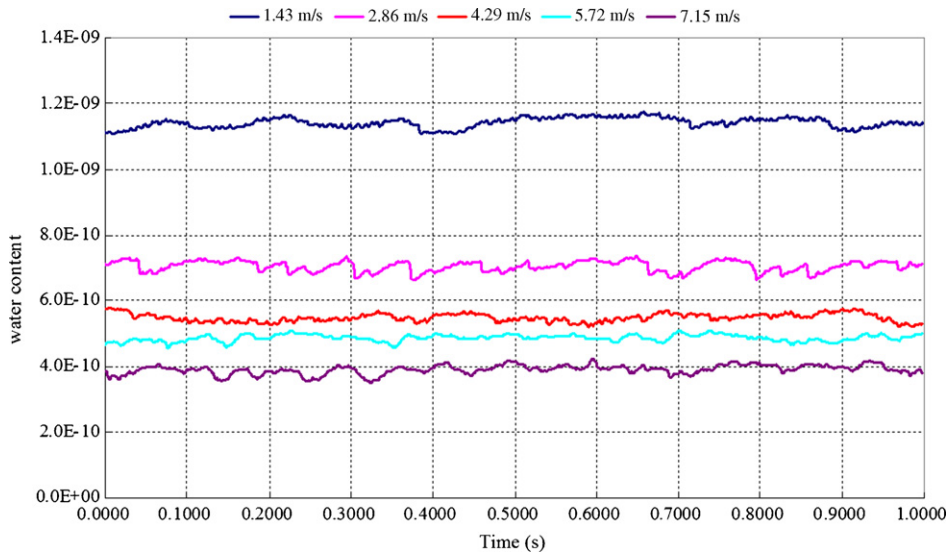

Fig. 18. Water content history for five cases involving different air inlet velocities.

droplet-merging, and the periodical corner flow along the upper outer edge, can be observed. The only difference is that the water moves more quickly to the channel exit compared with the case of 1.43 m s^{-1}. Correspondingly, less GDL surface is covered by the liquid water.

For the case of 4.29 m s^{-1} ($Re = 197$), the effects of interfacial tension become more significant, thus weakening the water accumulation—along the flow direction, only in the first upper corner can the water accumulation be observed. Besides, asymmetrical water distribution about the channel centerline on the GDL surface becomes visible—more water accumulating along the lower inner edge of the U-shaped channel than that along the lower outer edge. It is well known that an air flow cannot make a sharp turn due to its inertia, which causes an asymmetrically distributed air velocity in the after-bend area. This asymmetrical gas velocity distribution introduces asymmetrical interfacial tension, which eventually results in the asymmetrical water distributions in a cross-section normal to the centerline.

For the case when we increase the inlet velocity to 5.72 m s^{-1} ($Re = 263$), the asymmetry observed in the previous case is further enhanced. It can also be observed that most of the GDL surface has been cleaned up by the increasing shear force (or interfacial tension), which is obviously beneficial for reactant access to reaction sites. Another point which is worth mentioning is the compressing effects on the liquid recirculating zones by the air flow with increasing velocity: along the flow direction, the liquid recirculating zone at the second lower corner almost disappears while the one at the first lower corner has been greatly compressed and occupies only a small portion of the corner.

For the last case (7.15 m s^{-1} and $Re = 329$), the liquid recirculating zones at all sharp corners have been greatly compressed and none can be observed at the corners closed to the upper channel surface—the air flow with high velocity cuts off com-

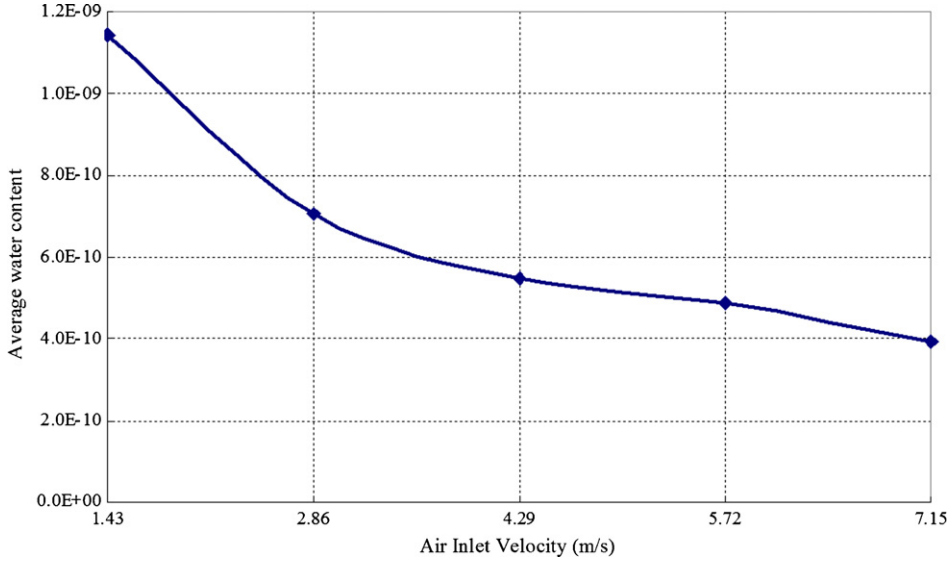

Fig. 19. Average water content vs. air inlet velocity.

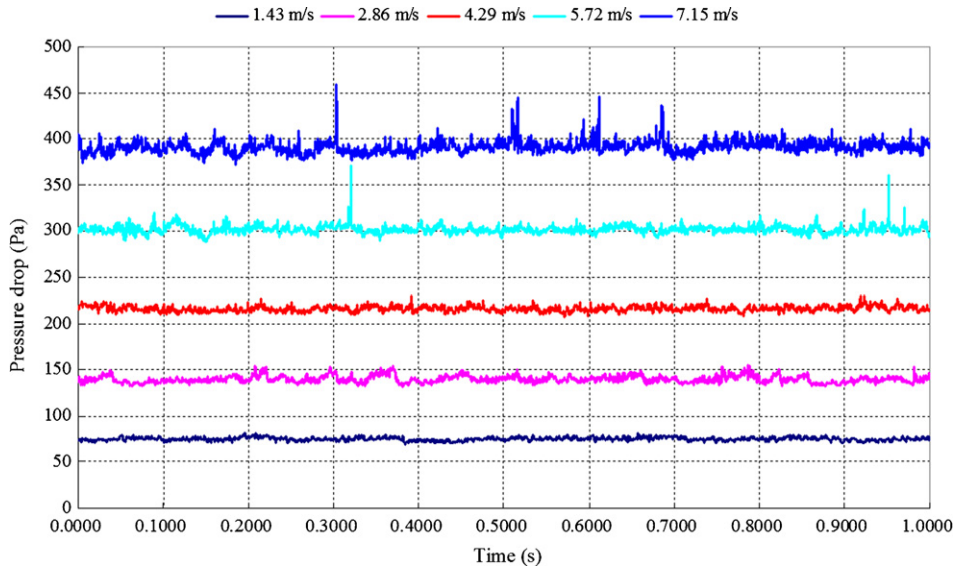

Fig. 20. Pressure drop history for five cases involving different air inlet velocities.

pletely the path for water to climb up onto the upper surface. In addition, the water movement along the lower edges becomes very fast and the corner flow becomes discontinuous, which could further increase the effective GDL area for reactant transport.

3.3.2. *Effects of inlet gas velocity on water content*

Fig. 18 shows the water content history for all the five cases (varying inlet velocities) within 1 s of the quasi-steady process. The fluctuation of water content with time can be clearly observed. The relationship between average water content and air inlet velocity is plotted in Fig. 19, in which the water content inside the gas flow channel decreases with increasing inlet velocity. Therefore, higher air inlet velocity may provide a better way for rapid and effective water removal. However, higher air inlet velocity means higher accessory power consumption. Thus the flow rate and timing must be optimized in the water management strategy.

3.3.3. *Effects of inlet gas velocity on pressure drop*

The plot of pressure drop history for the five cases is given in Fig. 20. It can be easily observed that, at lower inlet velocity, the pressure drop for the two-phase duct flow is quite stable. With increasing inlet gas velocity, the two-phase flow starts losing its stability and the high-amplitude oscillation can be readily captured. Besides, considering that the two-phase flow inside the gas flow channel is at relatively low velocity for all these cases, the overall flow regime is laminar. Similar to classical single-phase pipe or duct flow, in which the pressure drop is directly proportional to flow velocity, the relationship between pressure drop and velocity for this two-phase case is also nearly linear, as shown in Fig. 21. Careful observation reveals that the

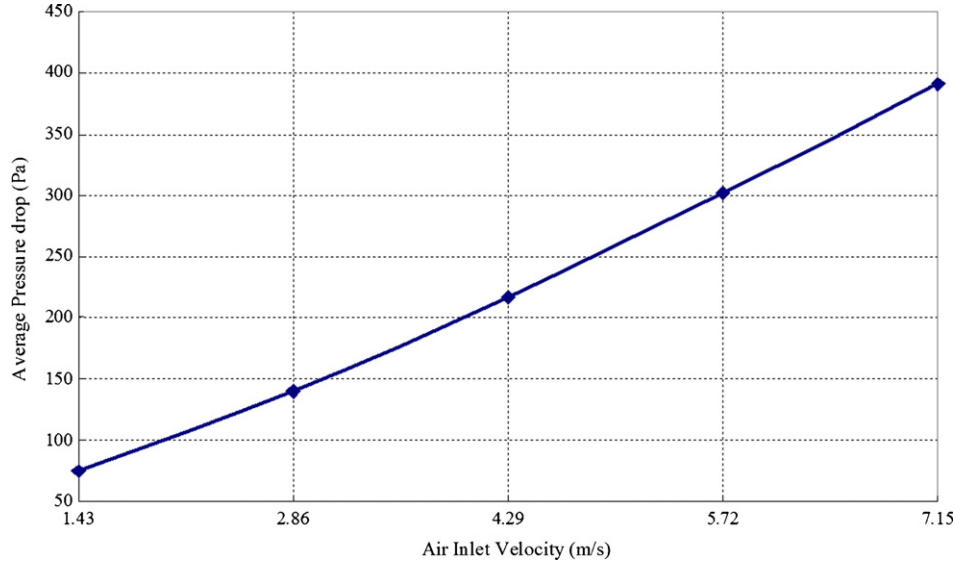

Fig. 21. Average pressure drop vs. air inlet velocity.

curve deviates from linear relation in the high velocity region. This might be caused by the strong interaction between the two phases, which introduces additional resistance to the air flow at high velocity.

4. Conclusions

(1) The hydrophilicity of reactant flow channel surface plays an important role in water management of a reactant flow channel—a hydrophilic surface could benefit the transport of reactants to the reaction sites by facilitating water transport along the channel edges or on the channel surfaces.
(2) Water content in the channel is at the highest when no wall adhesion is considered (or the contact angle is set to 90°), but it decreases with increasing air inlet velocity.
(3) Hydrophilic channel surfaces provide an effective water management strategy inside an air flow channel, but it would also introduce significantly higher pressure drop. This is caused by both blockage effect and wave drag effect introduced by the liquid water inside the gas flow channel.
(4) A sharp corner channel could be a better design option since a sharp corner could provide a space for water accumulation and paths for water to climb up onto upper surfaces, thus leaving more GDL surface area for reactant transport. And, compared with round corner channel, the increased pressure drop for the sharp corner channel design is negligible.
(5) Increasing inlet velocity could make the water distribution inside the channel reasonably good in term of water management. The corresponding pressure drop increases almost linearly, which is similar to a single-phase laminar case.

Acknowledgements

The support of Mr. Shinichi Hirano of Ford Motor Company, Ford University Research Program, and the Institute of Manufacturing Research at Wayne State University is greatly appreciated.

References

[1] S. Gottesfeld, Adv. Electrochem. Sci. Eng. 5 (1997) 195.
[2] T.E. Springer, T.A. Zawodzinski, S. Gottesfeld, J. Electrochem. Soc. 138 (1991) 2334.
[3] T.V. Nguyen, R.E. White, J. Electrochem. Soc. 140 (1993) 2178.
[4] J. Cao, N. Djilali, Trans. ASME 127 (2005) 26.
[5] S. Litster, D. Sinton, N. Djilali, Journal of Power Sources 154 (2006) 95–105.
[6] R. Satija, D.L. Jacobson, M. Arif, S.A. Werner, J. Power Sources 129 (2004) 238–245.
[7] P.A. Chuanga, A. Turhana, A.K. Hellera, J.S. Brenizera, T.A. Traboldb, M.M. Mench, Proceedings of the FUELCELL2005, May, 2005, pp. 23–25.
[8] J. Zhang, R. Shimoi, K. Shinohara, D. Kramer, E. Lehmann, G.G. Scherer, Proceedings of the 214th International Conference on the Properties of Water and Steam in Kyoto.
[9] D. Kramera, J. Zhang, R. Shimoic, E. Lehmann, A. Wokauna, K. Shinoharac, G.G. Scherer, Electrochim. Acta 50 (2005) 2603–2614.
[10] N. Pekula, K. Heller, P.A. Chuang, A. Turhan, M.M. Mench, J.S. Brenizer, K. Unlu, Nucl. Instrum. Meth. Phys. Res. A 542 (2005) 134–141.
[11] S. Tsushima, K. Teranishi, S. Hirai, Electrochem. Solid-State Lett. 7–9 (2004) A269–A272.
[12] S. Tsushima, T. Nanjo, K. Nishida, K. Teranishi, S. Hirai, 208th ECS Meeting, Abstract #930.
[13] K.W. Feindel, S.H. Bergens, R.E. Wasylishen, ChemPhysChem 7 (2006) 67–75.
[14] S. Li, U. Becker, Proceedings of the FUELCELL2004, June 14–16, 2005, pp. 157–164.
[15] D.M. Bernardi, M.W. Verbrugge, AIChE J. 37 (1991) 1151.
[16] D.M. Bernardi, M.W. Verbrugge, J. Electrochem. Soc. 139 (1992) 2477.
[17] F.Y. Zhang, X.G. Yang, C.Y. Wang, J. Electrochem. Soc. 153 (2) (2006) A225–A232.
[18] P. Quan, B. Zhou, S. Andrzej, Z. Liu, J. Power Sources 152 (2005) 131–145.
[19] FLUENT 6.2 User's Guide, FlUENT.
[20] K. Jiao, B. Zhou, P. Quan, J. Power Sources 154 (2006) 124–137.
[21] Z. Zhan, J. Xiao, M. Pan, R. Yuan, J. Power Sources, in press.
[22] J.S. Yi, T.V. Nguyen, J. Electrochem. Soc. 146 (1) (1999) 38–45.
[23] J.U. Brackbill, D.B. Kothe, C. Zemach, J. Comput. Phys. 100 (1992) 335.
[24] J.L. Liow, Proceedings of the 15th Australasian Fluid Mechanics Conference, The University of Sydney, Sydney, Australia, December 13–17, 2004.